Atmospheric Research 199 (2018) 209–223

Contents lists available at ScienceDirect

Atmospheric Research

journal homepage: www.elsevier.com/locate/atmosres

The response of a simulated mesoscale convective system to increased aerosol pollution: Part II: Derecho characteristics and intensity in response to increased pollution

Michal Clavner[a,*], Lewis D. Grasso[b], William R. Cotton[a], Susan C. van den Heever[a]

[a] Department of Atmospheric Science, Colorado State University, Fort Collins, CO, USA
[b] Cooperative Institute for Research in the Atmosphere, Colorado State University, USA

ARTICLE INFO

Keywords:
MCS
Straight-line winds
Derecho
Pollution aerosols

ABSTRACT

Mesoscale Convective Systems (MCS) are important contributors to rainfall as well as producers of severe weather such as hail, tornados, and straight-line wind events known as derechos. In this study, different aerosol concentrations and their effects on a derecho event are examined by simulating a case study, the 8 May 2009 "Super-Derecho", using the Regional Atmospheric Modeling System (RAMS), a cloud-resolving model with sophisticated aerosol and cloud microphysics. Three simulations were conducted that differed in the initial aerosol concentrations, spatial distribution and chemical composition as derived from output of GEOS-Chem, a 3D chemical transport model. In order to understand the impact of changes in aerosol concentrations on the derecho characteristics, the dynamical processes that produced the strong surface wind were determined by performing back-trajectory analysis during two periods of the simulated storm: the development and the onset of dissipation. A time dependent and non-monotonic trend was found between the intensity of the derecho and the increased aerosol concentrations that served as cloud condensation nuclei. During the formation period of the MCS, the non-monotonic trend was attributed to the microphysical impact of aerosol loading on the intensity of the cold pool; that is, the impact of aerosols on both the melting and evaporation rates of hydrometeors. The subsequent intensity changes within the cold pool modified the balance between the horizontal vorticity generated by the cold pool and that of the environment, thereby impacting the orientation of the convective updraft at the leading line. This, in turn, altered the primary flow that contributed to the formation of the derecho-strength surface winds. The simulation with no anthropogenic aerosols exhibited the strongest cold pool and the primary flow was associated with a descending rear inflow jet that produced the derecho winds over a larger region. The simulation with the highest amount of anthropogenic aerosols featured a stronger mesovortex and the derecho winds were primarily due to stronger convective downbursts. As the simulated storm matured, the changes in the derecho winds were found to be associated with the strength of the mesovortex at the gust front. During the period when the simulated storm began to dissipate, the non-monotonic trend in derecho intensity was associated with a non-monotonic response in mesovortex strength to increased aerosol concentrations. A moderate increase in aerosol concentrations led to the formation of a weaker mesovortex while a greater increase in aerosol concentration led to the formation of a stronger mesovortex. The formation of a stronger mesovortex was found to increase the contribution of the derecho winds following a convective downburst associated with an "up-down" downdraft trajectory.

1. Introduction

In the High Plains of the United States, Mesoscale Convective Systems (MCS) can produce potentially damaging straight line winds over a large region. The meteorological phenomenon of straight line winds was discovered by Hinrichs (1888), who named the phenomena "derecho", a Spanish word which can be interpreted as "straight ahead". Johns and Hirt (1987) reintroduced the term "derecho" to describe convectively induced severe wind as "any family of downburst clusters produced by an extratropical mesoscale convective weather system". Based on operational forecasting experience and the definition of a family of downburst clusters (Fujita and Wakimoto, 1981; Johns, 1982), Johns and Hirt (1987) set the criteria for a severe wind event to be classified as a derecho based on the following spatial, temporal, and

* Corresponding author.
E-mail address: michalcl@atmos.colostate.edu (M. Clavner).

http://dx.doi.org/10.1016/j.atmosres.2017.06.002
Received 3 January 2017; Received in revised form 26 April 2017; Accepted 2 June 2017
Available online 03 June 2017
0169-8095/

wind speed constraints:

- Concentrated area of reports consisting of convectively induced wind damage and/or convective gusts $\geq 26\ ms^{-1}$ (50 knots). This area must have a major axis length of at least 400 km. The severe wind events must be caused by the same MCS and show a pattern of chronological progression.
- Within the derecho area there must be at least three severe wind reports separated by 64 km or more of either 18–33 ms^{-1} and/or convective gusts of 33 ms^{-1} (65 knots) or greater.

In this paper derecho-strength (DS) winds will hereafter be referred to as DS winds. The criterion of "a pattern of chronological progression" refers to the following two types of derechos: progressive and serial. These two types are distinguished by the organization of an MCS, which produces the severe winds, as seen from radar reflectivity (Johns and Hirt, 1987). Radar signatures associated with downbursts and microbursts were identified and named "bow-echo" by Fujita (1978) due to the bowed appearance of the pattern of radar reflectivity. A bow-echo pattern evolves as a convective downdraft reaches the surface and creates an enhanced outflow, which subsequently propagates convective cells forward. Consequently, the apex of the bow signifies the location of the greatest wind speeds near the surface (Fujita, 1978).

Two primary dynamical processes have been identified to explain the formation of the surface outflow that constitutes a derecho. DS surface winds may result from (Adams-Selin et al., 2013) enhanced downdrafts due to negatively buoyant air, which is in response to melting and evaporation of precipitation (Fujita, 1978), and/or (Andreae et al., 2004) the transfer of high momentum air into the boundary layer (Newton, 1950) by a rear inflow jet (RIJ) (Smull and Houze, 1987). Convective features within an MCS, such as supercell-like convective cells were found to intensify a derecho by accelerating downdrafts that form due to the transport of negatively buoyant boundary layer air within an "up-down" downdraft (Knupp, 1987; Bernardet and Cotton, 1998) and intensifying the flow within a RIJ (Schmidt and Cotton, 1989). Another convective feature within an MCS that was found to produce DS surface winds are meso-γ-scale (2–20 km) mesovortices (Orlanski, 1975; Wakimoto et al., 2006; Atkins and St. Laurent, 2009a). An open question centers on potential dynamical changes in the above two processes in response to variations in concentrations of aerosol serving as cloud concentration nuclei (CCN).

Past numerical and observational studies have found that increased aerosol concentrations may lead to an invigoration of deep convective storms. Invigoration is due to the indirect effect of aerosols serving as Cloud Condensation Nuceli (CCN) (e.g. Andreae et al., 2004; Khain et al., 2005; van den Heever and Cotton, 2007; Lee et al., 2008; Rosenfeld et al., 2008; Fan et al., 2013; Storer and van den Heever, 2013). These studies have shown that when higher aerosol concentrations increase concentrations of CCN, smaller cloud droplets form leading to a reduction in the collision-coalescence efficiency. As a result, warm rain production is reduced; increased cloud droplet mass is transported vertically within an updraft, which then freezes homogeneously and releases additional latent heat that subsequently intensifies the updraft. Changes in aerosol concentrations have been found to impact both MCS precipitation and intensity (e.g. Khain et al., 2005; Tao et al., 2007; Li et al., 2009; Seigel and van den Heever, 2013; Lebo and Morrison, 2014; Saleeby et al., 2016) by altering the distribution and characteristics of hydrometeors within an MCS, specifically the diameter of hydrometeors. Changes in the diameter of hydrometeors directly impacts the potential for melting and/or evaporation of hydrometeors (van den Heever and Cotton, 2004; Bryan and Morrison, 2012; Adams-Selin et al., 2013; Storer and van den Heever, 2013) and, consequently, the intensity of cold pools (van den Heever and Cotton, 2004; Tao et al., 2007; Li et al., 2009; Seigel et al., 2013; Grant and van den Heever, 2015).

Variations in the intensity of a cold pool have been shown to alter other characteristics of an MCS. Adams-Selin et al. (2013) discussed the sensitivity of the structure and intensity of a simulated bow-echo to the intensity of a cold pools. Weisman (1992) showed the impact of cold pool intensity on the convective structure associated with a derecho event, as well as the intensity of a RIJ. Seigel and van den Heever, 2013 found that changes in hail size may introduce a positive feedback on RIJ intensity within a squall line via the recirculation of hydrometeors between the convective and stratiform regions. Cold pool intensity was also found to impact baroclinically generated horizontal vorticity within a cold pool, thereby impacting the balance between horizontal vorticity within a cold pool and that of the low-level (0–3 km) environmental wind shear at the leading line of an MCS: a central concept in RKW-theory (Rotunno et al., 1988). Changes in the balance between horizontal vorticity within a cold pool and the low-level environment were found to impact the intensity of the RIJ by altering the tilt of convective cores (Weisman, 1992, 1993) as well as the formation of mesovortices along an outflow boundary by modifying the amount of horizontal vorticity tilted into the vertical (Weisman and Trapp, 2003). An implication of the above studies is that the sensitivity of a derecho event to changes in aerosol concentrations will depend on the potential impacts that aerosols may have on the parent MCS, particularly cold pool intensity. In addition, the response of MCS morphology to aerosol impacts was also found to be dependent on characteristics of the environment such as humidity (Khain et al., 2005; Tao et al., 2007) and vertical wind shear (Fan et al., 2013; Lebo and Morrison, 2014). As a result, MCS behavior can change from one event to the next (e.g. Tao et al., 2007).

In this study, the impact of enhanced anthropogenic aerosols on the case study of 8 May 2009 "Super derecho" MCS is investigated. The derecho event of the 8 May 2009 storm has been analyzed in several past studies which focused on the environmental characteristics of the system (Coniglio et al., 2011, 2012; Keene and Schumacher, 2013). In addition, other studies concentrated on the development of meso-β (2–200 km) (Weisman et al., 2013; Evans et al., 2014), and meso-γ (2–20 km) vortices (Przybylinksi et al., 2010; Xu et al., 2015a, 2015b) in the 8 May 2009 MCS. This study adds to the current body of work by examining the impacts of increased anthropogenic aerosol concentrations on the characteristics of this system. In part I (Clavner et al., 2015; hereafter referred to as Part I), the impact of increasing aerosol concentrations that can serve as CCN were found to lead to stronger updrafts, enhanced convective precipitation, and a decrease in stratiform precipitation. This paper is organized as follows: the 8 May 2009 case study is presented in Section 2 while the model set up and aerosol sensitivity tests are given in Section 3. The results of changing aerosol concentration on the simulated 8 May 2009 derecho are presented in Section 4. A discussion and conclusions are given in Sections 5 and 6, respectively.

2. The 8 May 2009 MCS

Several previous studies have examined many different aspects of the 8 May 2009 MCS. In particular, this event has been characterized as a leading-line (Coniglio et al., 2011; Weisman et al., 2013), trailing stratiform (Houze et al., 1989; Parker and Johnson, 2000) bow-echo (Fujita, 1978) MCS, which developed a warm-core meso-β-scale (20–200 km) vortex in its later stage (Weisman et al., 2013; Evans et al., 2014), as well as several meso-γ-scale (2–20 km) vorticies (Xu et al., 2015a, 2015b). The MCS developed in western Kansas at ~0600 UTC and moved south-southeastwards to the southern Appalachians, traveling over a thousand miles before dissipating at 1900 UTC (Coniglio et al., 2011; Storm Prediction Center (SPC)). Unique environment characteristics that aided in the genesis and longevity of the 8 May 2009 MCS included a strong Low Level Jet (LLJ) and anomalously large values of precipitable water (PW) content along an east-west oriented surface boundary (Coniglio et al., 2011). A more detailed description of the MCS environment, structure and propagation is found in Part I. DS

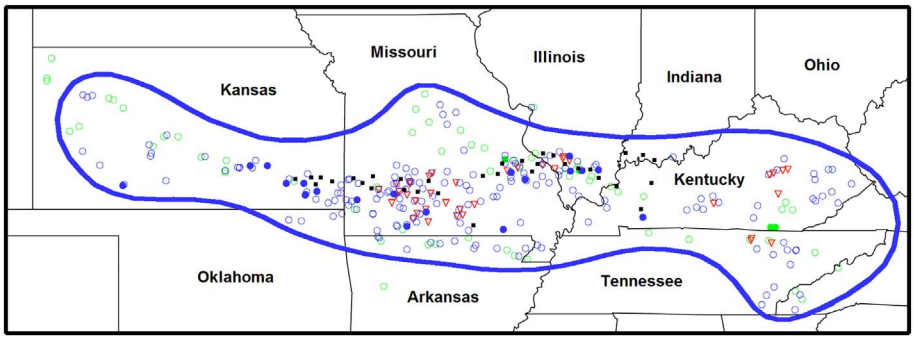

Fig. 1. The area affected by the May 8, 2009 "Super Derecho" convective system and the severe weather reports associated with it (www.spc.noaa.gov). Area affected is outlined in blue. Severe reports are for the period from 0300 to 2300 UTC May 8, 2009. Wind damage or wind gusts ≥ 50 kts (58 mph) (open blue circles); estimated or measured wind gusts ≥ 65 kts (74 mph) (filled blue circles); hail ≥ 0.75 in. (open green circles); hail ≥ 2.0 in. (filled green circles); and tornados (red triangles) are all shown. Flash flooding (by county) is denoted by black squares. Area of most intense wind damage is approximated by band of filled blue circles extending from southeast Kansas through southern Missouri into southern Illinois. (For interpretation of the references to colour in this figure legend, the reader is referred to the web version of this article.)

winds that were produced by the 8 May 2009 MCS occurred along the entire storm track, from western Kansas to the region where the system dissipated, west of the Appalachians (Fig. 1). As the storm moved from Kansas into Missouri, a large scale bow-echo developed and several cyclonic meso-γ vortices formed near the apex of the bow-echo on the low-level convergence zone (Przybylinksi et al., 2010). Analysis of reflectivity and Doppler velocity over southwest Missouri showed that the meso-γ vortices occurred simultaneously at ~1330 UTC and that the strongest meso-γ vortex formed in the region where the cold pool and low level shear were balanced, resulting in vertically-erect towers (Przybylinksi et al., 2010). The evolution of the meso-γ vortices within the 8 May 2009 MCS was examined numerically by Xu et al. (2015a, 2015b) and were found to form at the leading line of the bow-echo, similar to the observational findings of Przybylinksi et al. (2010).

As the storm matured, the northern end of the bow echo occluded forming a warm core meso-β vortex (Weisman et al., 2013; Evans et al., 2014) that was apparent in radar imagery as a comma shape echo (see Fig. 1f, Part I). During the evolution of the meso-β vortex (~1700 UTC), the cold pool associated with the MCS weakened. As a result, strong surface winds developed in response to the deepening and intensification of the meso-β vortex to the surface rather than the cold pool forcing (Weisman et al., 2013; Evans et al., 2014).

In summary, the 8 May 2009 MCS, DS winds were found to be generated due to enhanced convective downdrafts, in association with the storm generated cold pool and a descending RIJ. Furthermore, strong surface winds were found to be enhanced due to the formation of meso-γ vortices along the gust front and in association with a warm core meso-β vortex that formed during the later stages of the 8 May 2009 MCS. These past studies show that there are several different dynamical processes that may be responsible for the formation of DS surface winds. The impact of changes in aerosol concentration on these processes is the focus of this study.

3. Numerical model and experiment setup

3.1. Model configuration

The 8 May 2009 MCS case study was simulated using the Colorado State University Regional Atmospheric Modeling System (RAMS) version 6 (Cotton et al., 2003; Saleeby and van den Heever, 2013). The RAMS model simulation was configured as a heterogeneous, cloud resolving mesoscale model with three interactive grids (see Fig. 4, Part I). Grids 1 and 2 were set up with a horizontal grid spacing of 40 and 8 km, respectively. The finest nested grid was set up with a horizontal grid spacing of 1.6 km and covers the entire region of the simulated MCS from genesis to decay. Detailed information on the RAMS model setup is described in Section 3.1 of Part I.

3.2. RAMS simulations

In order to examine the impact of increased aerosol concentrations on the derecho characteristics of this simulated MCS, a set of three numerical simulations was performed: CLEAN, POLLUTED, and 5xPOLLUTED. As described in Section 3.1, the three simulations utilized the same RAMS model configuration with the exception of their initial aerosol concentrations and spatial distribution. Aerosol concentrations were derived from GEOS-Chem (Bey et al., 2001), a 3D global chemistry model. Additional details about GEOS-Chem, output from GEOS-Chem, and the method of implementation of aerosols with RAMS are found in Part 1. Fig. 5 (Part I) presents the vertical profiles of the average total aerosol concentrations [cm^{-3}] at the time of genesis of the MCS (0630 UTC) in the three different RAMS simulations. The CLEAN and POLLUTED simulations were initialized with aerosols derived from only natural emissions (no anthropogenic sources), and both natural and anthropogenic emissions, respectively. The 5xPOLLUTED simulation was initialized with the same aerosol distribution as the POLLUTED simulation, except that both aerosol mass and concentrations were multiplied by a factor of five in order to examine the impacts of a highly polluted scenario.

3.3. Back trajectory analysis

In order to understand the impact of changes in aerosol concentrations on the derecho characteristics, dynamical processes that produced the simulated DS winds were first determined. Dynamical processes in this study were analyzed by computing back-trajectories (BT) with a Lagrangian model (LM) (Grasso, 1996) from grid points with DS winds for all three RAMS simulations. Grid points with DS winds were determined according to the surface wind speeds at the second vertical model level above ground level (~75 m AGL). Wind speed magnitudes of at least 26 ms^{-1} were considered to be part of the simulated derecho event, following the minimum wind speed criteria set by Johns and Hirt (1987).

For each of the three simulations, RAMS was rerun for 60 min for different periods of the storm. During each 60 min time period, the components (u, v, and w) of the 3D wind, virtual potential temperature, and the total condensate mixing ratio were extracted from the Eulerian RAMS Grid 3 at each time step (3.33 s). Values of the extracted variables were then transferred, by a tri-linear spatial interpolation scheme within the LM to the parcel's location. Advection of a parcel was accomplished with the use of the 4th order Runge-Kutta method and a time step of 3.33 s, corresponding to the output time of RAMS velocity data: Interpolation in time was not needed.

The BTs were analyzed, along with various instantaneous fields extracted from RAMS every 30 min (output time interval of Grid 3 data for all three simulations) around the location of a parcel including budget tracking of microphysical processes and cold pool characteristics. The number of BT performed for each RAMS simulation depended on the number of grid points with DS winds and varied from 50 to 300.

4. Simulation results

In all three RAMS simulations, convective elements not directly

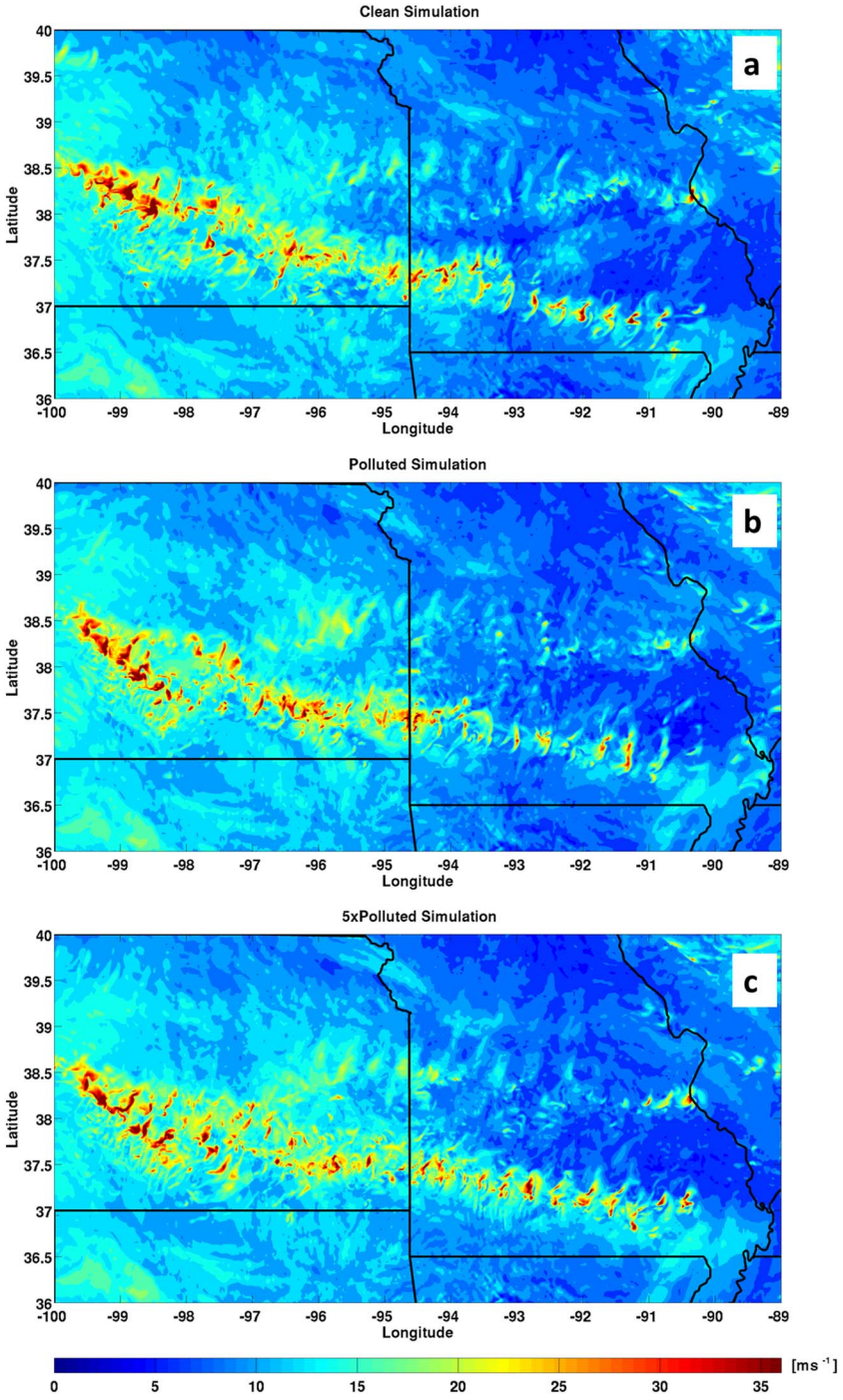

Fig. 2. Maximum surface wind speed [ms^{-1}] of the simulated MCS every 30 min during the analysis period (0630–1730 UTC) for the three simulations: (a) Clean, (b) Polluted and (c) 5xPolluted.

associated with the MCS also developed in Grid 3. In order to isolate the DS winds produced by the simulated 8 May 2009 case study, data from the other convective elements were numerically filtered out. The filtering technique, described in detail in Section 3.1 of Part I, incorporated parameters outputted every 30 min such as estimated cloud top temperature [C], precipitation rate [mm hr^{-1}] and vertically-integrated total condensate [kg m^{-2}]. In this study, data analyzed from the RAMS simulated MCS were taken from MCS genesis at 0630 UTC until 1730 UTC, after which the method for isolating the MCS was less reliable due to the dissipation of the system and subsequent fragmentation of the MCS' stratiform-anvil, as well as the close proximity of the storm to neighboring convection.

In order to assess the simulated derecho event, a map of surface wind magnitudes during the entire analysis period is presented in Fig. 2, for each of the three RAMS aerosol sensitivity simulations: CLEAN (Fig. 2a), POLLUTED (Fig. 2b) and 5xPOLLUTED (Fig. 2c). Each figure contains the maximum wind speed at each output time (30 min) during the analysis period (0630–1730 UTC) superimposed on the same figure in order to represent a map of the simulated derecho event as a function of space and time. All three of the simulations produced swaths of DS surface winds along a corridor from west Kansas progressing south southeastwards through southeast Kansas and the southern portion of Missouri. These cumulative maps compared favorably with the locations of the SPC reports of wind speeds > 50 knots (26 ms^{-1}) (Fig. 1) during 8 May 2009. A detailed comparison of the simulated MCS's formation, location and structure to observations is given in Section 4.2 of Part 1.

Changes in the simulated derecho characteristics as a result of

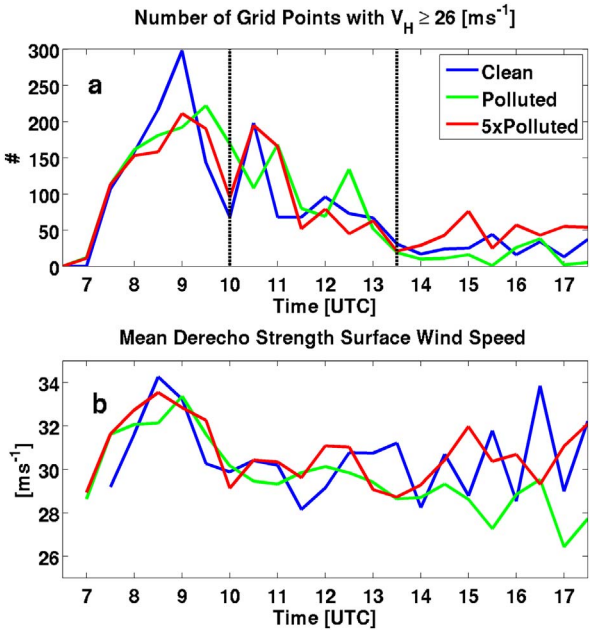

Fig. 3. Simulated (a) number of grid points with DS wind and (b) mean DS wind speed as a function of time for the Clean (blue), Polluted (green) and 5xPolluted (red) simulations. The dashed vertical lines, in 3a indicate the division of the MCS simulation in time to the three stages: intensification, mature and dissipation. (For interpretation of the references to colour in this figure legend, the reader is referred to the web version of this article.)

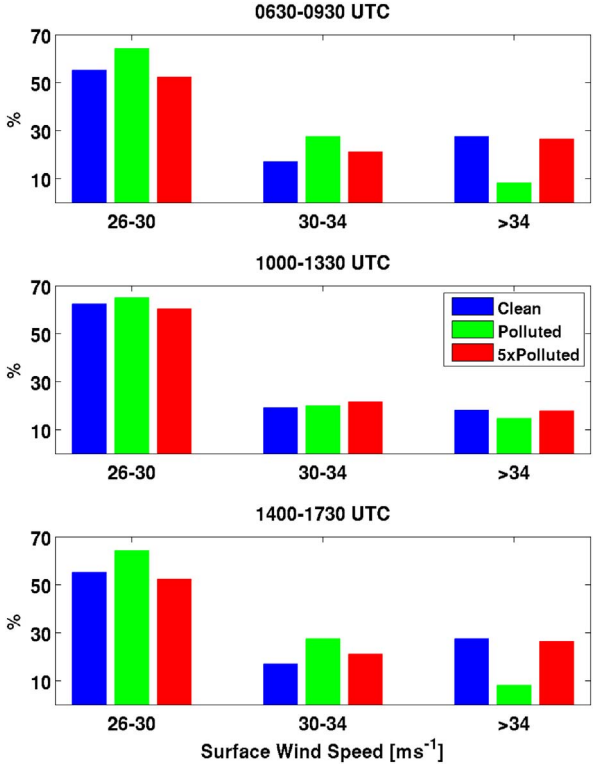

Fig. 4. Normalized distribution of DS wind speeds for the Clean (blue), Polluted (green), and 5xPolluted (red) simulations during (a) the intensification stage 0630–0930 UTC, (b) the mature stage 1000–1330 UTC, and (c) the dissipation stage 1400–1730 UTC. (For interpretation of the references to colour in this figure legend, the reader is referred to the web version of this article.)

variations in aerosol concentrations are now investigated. Two metrics are used to quantify the intensity of the simulated derecho during the analysis period (0630 and 1730 UTC): the number of grid points with DS wind and the magnitude of the DS wind speed (Johns and Hirt, 1987). A quantitative comparison of these two metrics among the three RAMS simulations are presented in Fig. 3. From the analysis of the number of grid points with DS winds over time, three stages within the simulation are apparent: intensification, mature and dissipation. During the intensification stage of the MCS, the area with DS wind was the largest and decreased with time as the storm matured and began to dissipate. This suggests that within each of the simulations, different mechanisms may be responsible for the generation of the DS winds as the MCS matured and weakened. Unlike the changes in the number of grid points with DS winds (Fig. 3a), the mean DS wind speed for both the CLEAN and 5xPOLLUTED simulations are similar throughout the analysis period (Fig. 3b). Only the POLLUTED simulation shows a decrease in mean DS wind speeds as a function of time. This is discussed in Section 4.2.

The intensity of the DS winds was further investigated by calculating the normalized distribution of the DS wind magnitudes during different periods of the storm: intensification (0630–0930), mature (1000–1330 UTC) and dissipation (1400–1730 UTC). The normalized distribution within three ranges of DS winds were examined corresponding to the DS minimum threshold wind speed (26 ms^{-1}) and the stronger DS gusts (34 ms^{-1}) (Johns and Hirt, 1987) in intervals of 4 ms^{-1} defined here as: weak (26–30 ms^{-1}), moderate (30–34 ms^{-1}) and strong (34 > ms^{-1}). The bin count was normalized by the total number of grid points with DS winds within each simulation for the three periods (Fig. 4). During the intensification stage of the MCS (Fig. 4a), a monotonic trend is apparent where increasing aerosol concentrations lead to stronger DS winds (Fig. 4a) over a smaller area (Fig. 3a). The increase in DS wind strength is evident through the decrease in the percentage of grid points within the weak DS wind category and an increase in the strong DS category (Fig. 4a). That is, the percentage of grid points in the weak bin decreases from the CLEAN (49%), POLLUTED (~47%) to the 5xPOLLUTED case (42%). However, in the strong bin, the percentage of grid points increases from the CLEAN (31%), POLLUTED (33%) to the 5xPOLLUTED case (37%).

During the mature stage (Fig. 4b) the intensity of the DS winds slightly decreases for the POLLUTED simulation, as seen by a higher bin count within the weak category, however, this decrease is even more prevalent within the dissipation stage (Fig. 4c). Within the POLLUTED simulation both the area of DS winds and the strength of DS winds decrease with time (Figs. 3b and 4c). Therefore, within the dissipation stage, an increase in aerosol concentration led to a non-monotonic trend in the derecho intensity since only the moderate increase in aerosol concentrations was found to weaken the derecho. The percentage of grid points in the weak bin for the POLLUTED (64%) simulation was the highest in comparison to the CLEAN (55%) and 5xPOLLUTED case (52%) and the lowest (8%) within the strong bin in comparison to 27% and 26% for the CLEAN and 5xPOLLUTED, respectively.

Among the three simulations, the differences between both area and intensity occurred primarily within both the intensification (Figs. 3a and 4a) and dissipation time periods (Figs. 3b and 4c). As a result, additional analysis was performed by conducting a 60 min BT analysis for the three simulations, during these times. BT analysis facilitates a time continuous examination on a finer time scale, in comparison to the instantaneous snapshots every model output time, of the air flow that generates the DS winds at the surface during these time periods. Thereby an examination of this flow among the three simulations permitted a detailed diagnosis of the dynamics responsible for generation of the DS winds within each simulation and the impacts of changes in aerosol concentrations on the flow. Findings of the derecho characteristics and results from BT analysis are presented in the following sections.

4.1. Simulated derecho at 0900 UTC: intensification stage

During this time, the dominant region with DS winds occurred in all

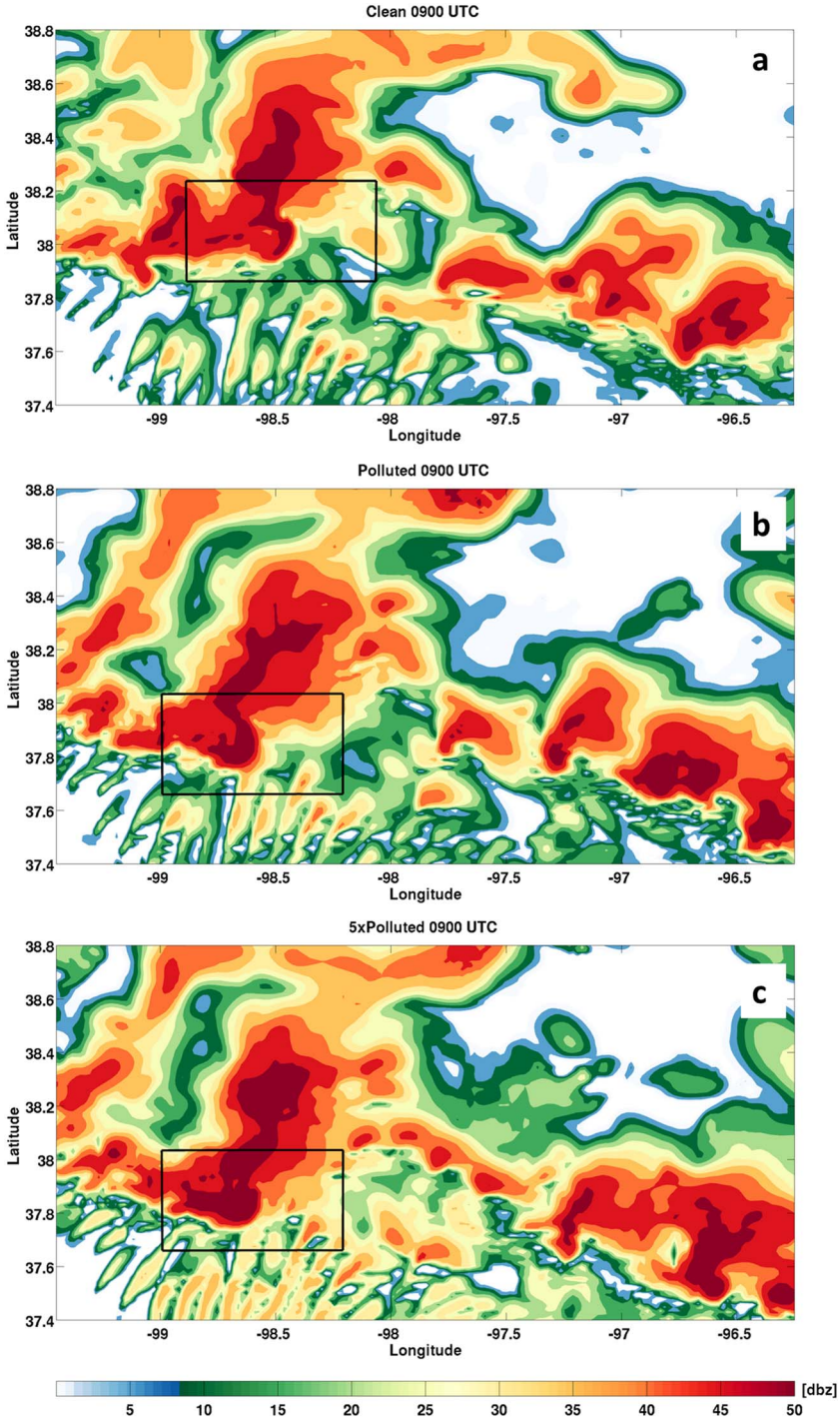

Fig. 5. Simulated radar reflectivity at 1 km at 0900 UTC for the three simulations: Clean (a), Polluted (b) and 5xPolluted (c). The analyzed region is enclosed within a black rectangle.

three simulations within the upstream region of the convective line in association with a Cell Bow Echo (Klimowski et al., 2004) that was embedded within the bowed convective line. Cell Bow Echoes are described as strong thunderstorms on the scale of 10–25 km which have bowed out due to strong outflow (Klimowski et al., 2004). The region with DS winds (boxed area in Fig. 5) is at the gust front portion of the Cell Bow Echoes. Fig. 6 presents the density potential temperature within the boxed are in Fig. 5. The relative difference between the cold pool density potential temperature (Emanuel, 1994) and that of the environment is a measure of cold pool buoyancy (Tompkins, 2001; Seigel et al., 2013). It is also a useful indication of the location of the gust front of the storm (Charba, 1974). Fig. 6 also shows area with DS winds (contoured in red), and the initialization location of the back-trajectory (BT) parcel locations within the three RAMS simulations: CLEAN, POLLUTED and 5xPOLLUTED.

The BT flow is presented in Figs. 6c, 7c and 8c for the CLEAN, POLLUTED and 5xPOLLUTED simulations as a function of location, as well as the parcels' horizontal velocity along its trajectory. The BT airflow shows that the DS winds originated from two main upper-level flows: a descending RIJ and an up-down downdraft (UDD). The importance of these two flows in the generation of the strong surface winds differs among the simulations, as determined by the fraction of the BT that followed each of the two flows. The dominant BT airflow in the CLEAN simulation was the RIJ (Fig. 6c), which accelerated toward the leading convective line at higher elevations (~3000 m AGL) than the RIJ in the POLLUTED (Fig. 7c) and 5xPOLLUTED (Fig. 8c)

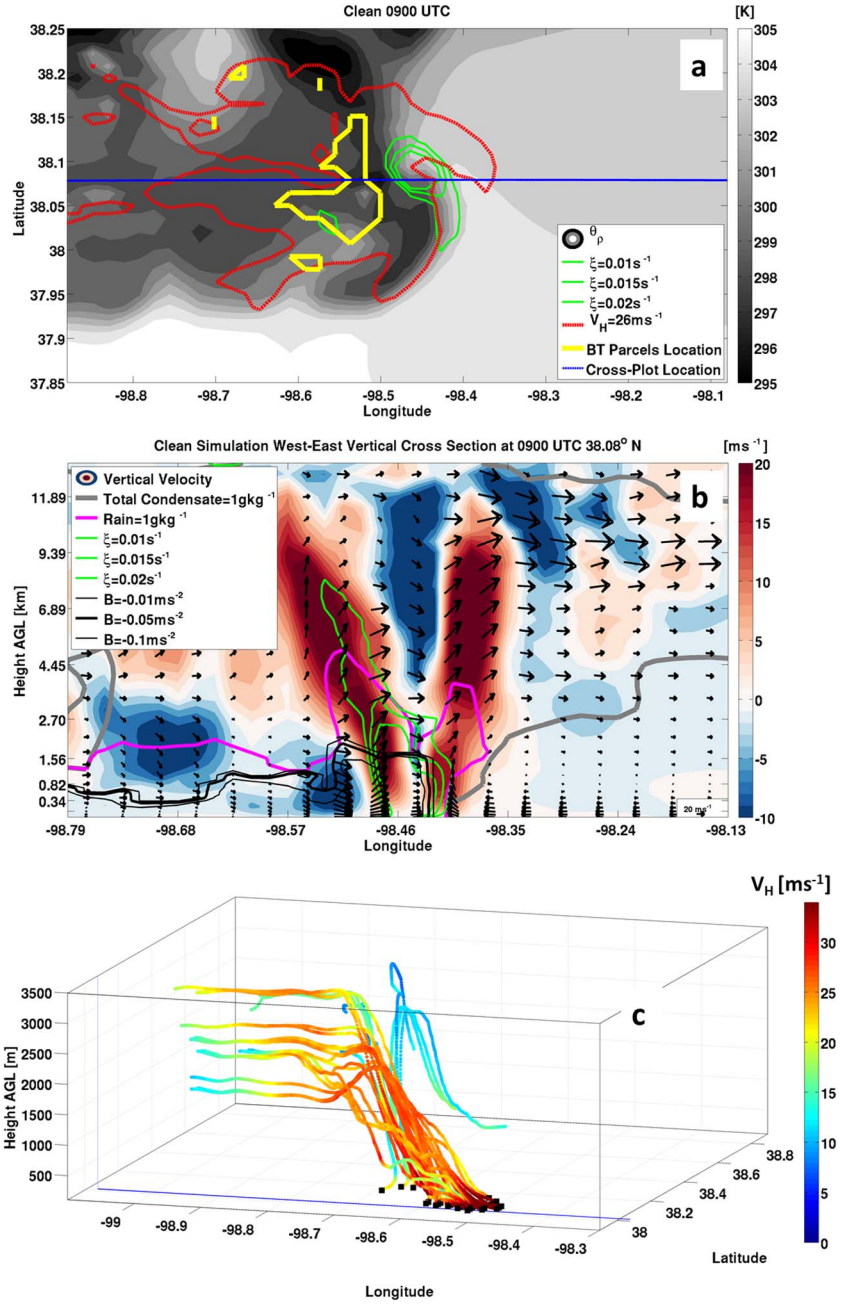

Fig. 6. Clean simulation at 0900 UTC: (a) Surface density potential temperature θρ [K] (shaded) of the area enclosed by the black rectangle in Fig. 5a. Superimposed are contours of vertical relative vorticity at 1 km AGL ($0.01\ s^{-1}$, $0.015\ s^{-1}$ and $0.02\ s^{-1}$ isopleths) representing the location of the meso-γ vortex at the gust front (green contours). The area with DS winds is contoured in red and the region with the location of the back trajectories analyzed contoured in yellow. Only back trajectories that descended above ground level were analyzed. The blue line across the figure presents the location of the cross plot within figure b. The location of this cross section was chosen along the mean location of the DS winds at the gust front. (b) Vertical cross section along the blue line shown in figure (a) of the vertical velocity [ms^{-1}] (shaded), with the (u, w) wind vectors and the meso-γ vortex represented in green contours of $0.01\ s^{-1}$, $0.015\ s^{-1}$ and $0.02\ s^{-1}$ relative vertical vorticity isopleths. The outline of the system is represented by the $1\ g\ kg^{-1}$ contour of the total condensate (grey) and the precipitation by the $1\ g\ kg^{-1}$ rain mixing ratio isopleth (magenta). The gust front is represented by the buoyancy value (b) of the cold pool contoured in black, as calculated according the density potential temperature. The edge of the cold pool is defined according to the isopleth of $-0.05\ ms^{-2}$, a value representative of mid-latitude cold pools (Seigel et al., 2013). Additional buoyancy value of $-0.01\ m\ s^{-2}$ and $-0.1\ m\ s^{-2}$ are also plotted to show the cold pool magnitude. (c) 30 min back trajectories (a sample size of 30) of the parcels within the region contoured in thicker red (figure a) and their relative location to the cross plot (figure b) (represented by the blue contour).The trajectories are colored according to the horizontal wind speed of the parcel along the trajectories. The vertical extent of the plot is 3500 m AGL. (For interpretation of the references to colour in this figure legend, the reader is referred to the web version of this article.)

simulations. In the 5xPOLLUTED simulation (Fig. 8c), the dominant flow consisted of an UDD. The UDD air originated near the surface east (upstream) of the storm, slowly ascended with weak vertical velocities (~4–7 ms^{-1}) (not shown) toward the leading convective cell, turning cyclonically and then rapidly descending (Fig. 9c) as the parcels encounter the precipitating downdraft on the upstream side of the convective updraft (Fig. 8c). The cyclonic turn of the parcels as they entered the leading convective line is explained by the meso-γ vortex (contoured in green, Fig. 8c), indicated by a volume of relative vertical vorticity > $0.01\ s^{-1}$ (Weisman and Trapp, 2003). A third flow in addition to the RIJ and UDD flow is also apparent in the 5xPOLLUTED simulation. This flow originated at 4 km AGL from the south-south west and is similar to the midlevel downdraft branch described in Knupp (1987). Within the POLLUTED simulation (Fig. 7c), BT flow indicates that both the RIJ and the UDD contributed in the formation of the DS winds.

A comparison of all the BT flows during the parcel's descent to the surface, for all three simulations is presented in Fig. 9 and compares the mean downdraft speed, horizontal speed, total condensate mixing, and virtual potential temperature. Fig. 9 shows that increasing the aerosol number concentration leads to a shift in the dominant BT flow from a prevalent RIJ in the CLEAN simulation, categorized by the stronger horizontal velocities at higher levels (Fig. 9d) to a dominant UDD flow within the 5xPOLLUTED simulation, defined by stronger downdraft speeds (Fig. 9c) which reach downburst intensities of greater than $-10\ ms^{-1}$ (Fujita, 1978). The shift in the BT flow from the RIJ to the UDD with increased aerosol pollution is explained by the response of the convection orientation at the gust front to aerosol-induced changes in the cold pool characteristics produced by the storm, following the RKW theory (Rotunno et al., 1988). A stronger RIJ forms when the main convective updraft is tilted upshear, forming a horizontal vorticity gradient between that of the cold pool and the tilted updraft (Weisman, 1992), as seen for the CLEAN simulation (Fig. 6b). A stronger meso-γ vortex will develop when the horizontal vorticity generated by the cold

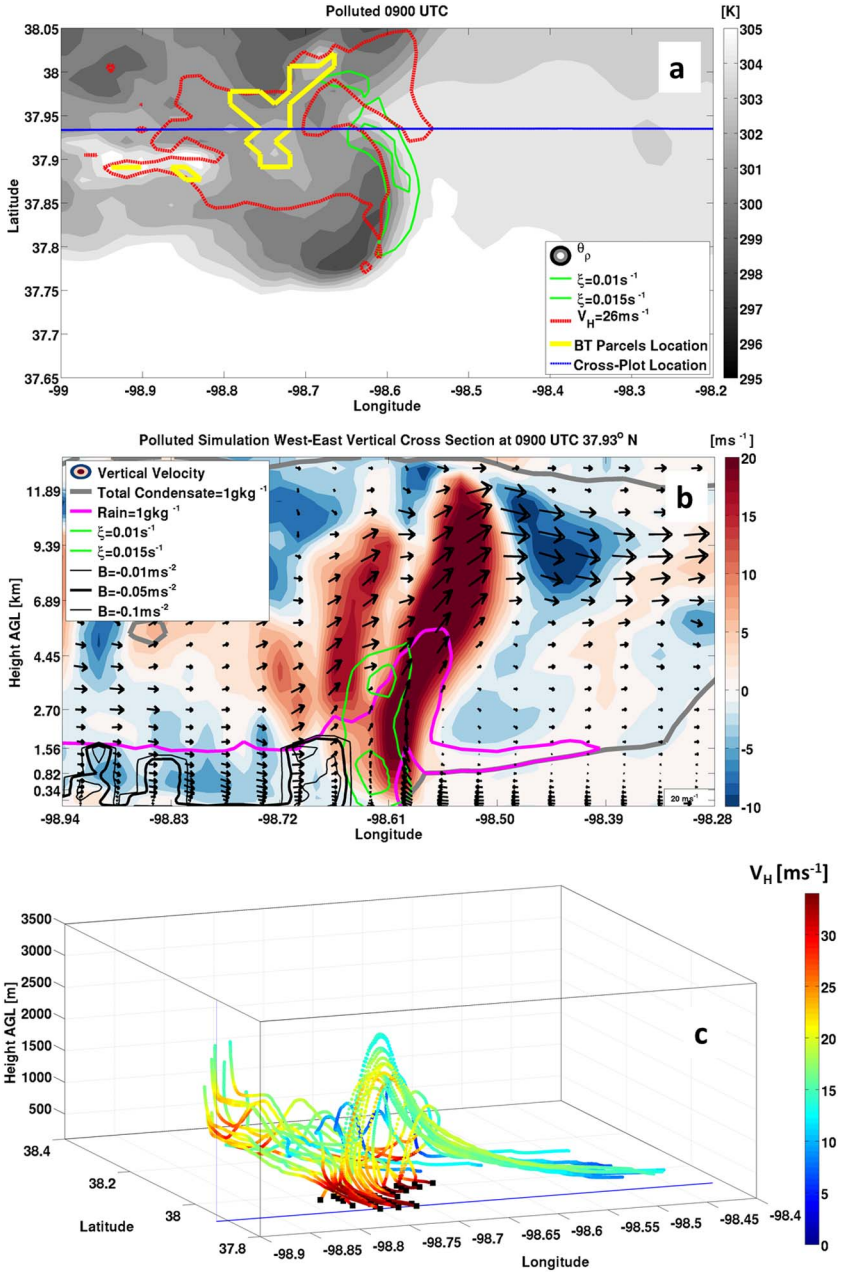

Fig. 7. Same as Fig. 6, for the Polluted simulation at 0900 UTC.

pool is in balance with that of the environmental shear (Atkins and St. Laurent, 2009b), leading to a more upright updraft, as seen in the 5xPOLLUTED simulation (Fig. 8b). Such a balanced state promotes the generation of relative vertical vorticity by the tilting of horizontal vorticity into the vertical as well as by stretching of the vortex tube (Atkins and St. Laurent, 2009b).

An increase in aerosol number concentration led to a non-monotonic trend within the cold pool temperature, indicated in the BT virtual potential temperature (Fig. 9f) as well as the surface plots of the density potential temperature (Fig. 6a, 7a and 8a). Changes in aerosol number concentrations were found to alter the strength of the cold pool (both temperature and depth) due to the changes they induce in the precipitating hydrometeor characteristics. In part I, we found that at this time, higher aerosol number concentrations enhanced both cold and warm rain formation in the 5xPOLLUTED simulation and warm rain formation in the POLLUTED simulation, leading to higher precipitation rates and the formation of larger raindrops near the surface in both cases. Within the CLEAN simulation the precipitation rates as well as rain droplets diameters were found to be smaller in comparison to both the POLLUTED and 5xPOLLUTED simulations. Therefore, aerosol-induced changes in precipitation formation mechanisms impacted both the rates of evaporation and melting of the hydrometeors, which in turn, altered the cold pool strength.

Here the changes in precipitation and evaporation are seen by examining the mean total condensation mixing ratio (Fig. 9e) and mean virtual potential temperature (Fig. 9f) during the decent of the parcels to the surface. Fig. 9e indicates that below 1 km, condensate loss due to evaporation occurred in all three of the simulations, however, at different altitudes and with different magnitudes. In the CLEAN simulation, evaporation is most evident near the surface, while for the 5xPOLLUTED simulation, evaporation occurs throughout the entire 1 km AGL depth. In the POLLUTED simulation, the near constant value of mean condensate mixing ratio indicates that at this time, this simulation exhibited the least amount of evaporation, and therefore, least amount of cooling within the downdraft in comparison to CLEAN and 5xPOLLUTED. Due to the enhanced precipitation formation in the

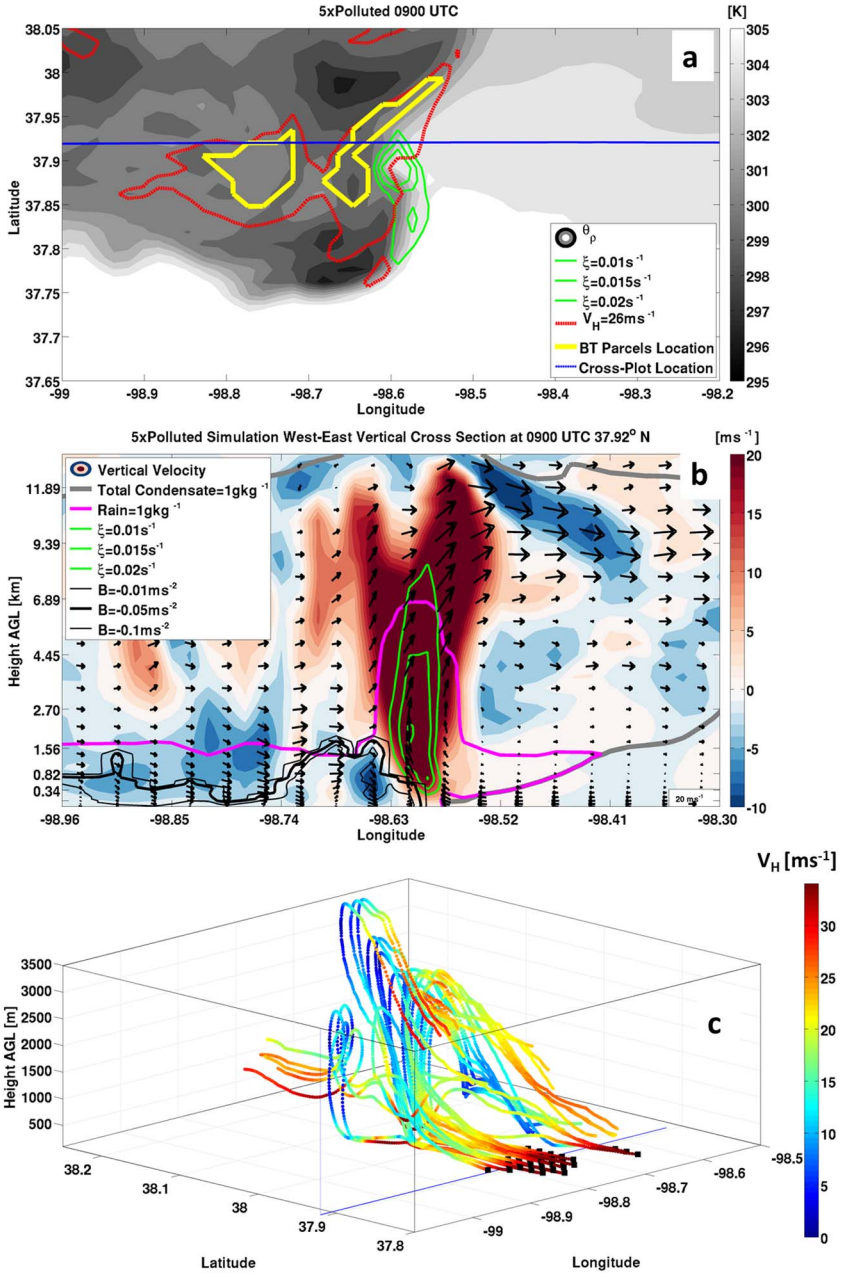

Fig. 8. Same as Fig. 6, for the 5xPolluted simulation at 0900 UTC.

5xPOLLUTED simulation, more mass was available to be evaporated at lower levels. However, the smaller raindrops (Part 1, Fig. 14a) within the CLEAN simulation increased the evaporation rates. The downdrafts were the warmest in the POLLUTED simulation (Fig. 9f) due to a decrease in evaporation, as seen in the near constant value of mean total condensate below 1 km AGL (Fig. 9e), indicating smaller amounts of total condensate loss within the downdraft in comparison to both CLEAN and 5xPOLLUTED (Fig. 9e). This decrease in evaporation is explained by both larger raindrops as well as smaller rain rates in the POLLUTED case in comparison to the 5xPOLLUTED simulation. Within the CLEAN simulation, the higher evaporation rates, in comparison to both the simulations with higher aerosol concentrations, impacted the cold pool strength by decreasing its density potential temperature and thus, increasing the horizontal gradient in density potential temperature between the cold pool and the environment and hence it's negative buoyancy and strength (Tompkins, 2001).

The orientation of the convection at the leading line shows that in the CLEAN simulation, for which the cold pool is the strongest, the updraft is tilted upshear which results in the BTs being predominantly from the RIJ (Fig. 6b). For the 5xPOLLUTED simulation, the cold pool is slightly weaker in comparison to the CLEAN simulation, leading to a more upright convective updraft (Fig. 8b), which enhanced the intensity of the meso-γ vortex. In the POLLUTED simulation, the cold pool was the weakest of the three simulations at 0900 UTC, and the convection at the leading line is seen to be tilted downshear. This limited the amount of vertical vorticity generated by stretching and produces a weaker meso-γ vortex (Fig. 7b). Despite the weaker cold pool and the shallower meso-γ vortex in the POLLUTED simulation, the downdraft speeds within the UDD were comparable to that of the 5xPOLLUTED simulation, emphasizing that the accelerations contributing to the stronger downdrafts in the former occurred at levels below 2 km AGL, consistent with the characteristics of an UDD (Knupp, 1987). The shift of the BT flow from a RIJ (CLEAN) to a UDD associated with the meso-γ vortex (5xPOLLUTED) explains why DS winds were stronger and occurred over a smaller region at 0900 UTC for the more polluted simulations.

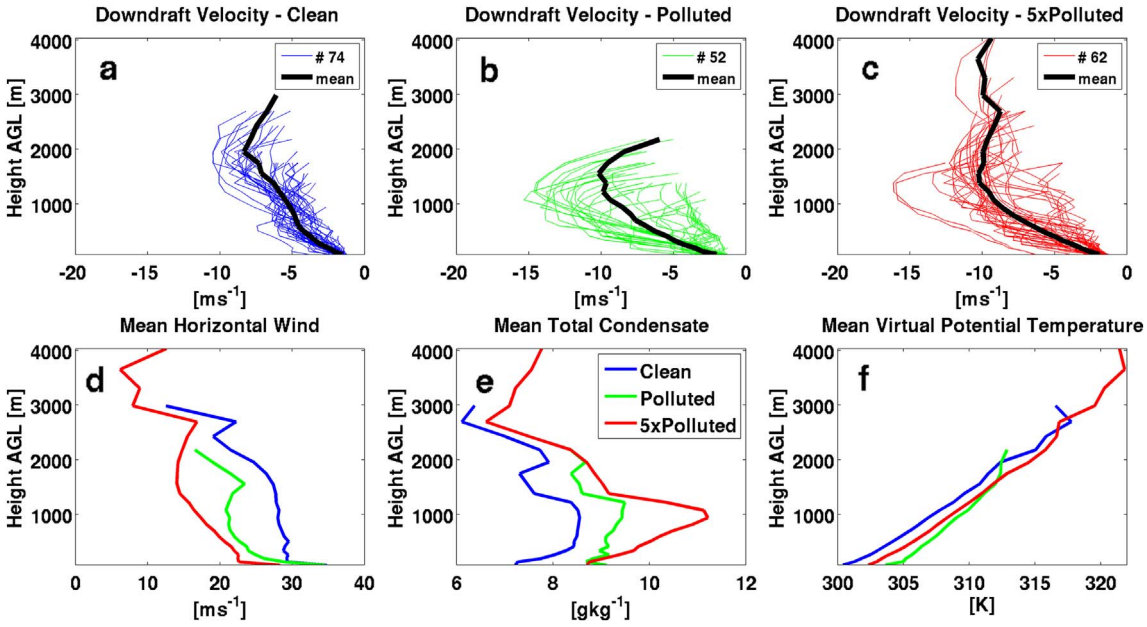

Fig. 9. Downdraft vertical velocity as a function of height for individual descending parcels that follow either the RIJ or the UDD and the mean vertical velocity for the Clean (a), Polluted (b) and 5xPolluted (c) back trajectory analysis. The number in parenthesis represents the number of parcels. Mean characteristics of the descending parcels of horizontal wind speed [ms^{-1}] (d), condensate loading [$g\ kg^{-1}$] (e) and mean virtual potential temperature [K] (f) for the Clean (blue), Polluted (green) and 5xPolluted (red) simulations are plotted as a function of height for the downdraft trajectories. (For interpretation of the references to colour in this figure legend, the reader is referred to the web version of this article.)

4.2. Simulated derecho at 1500 UTC: dissipation stage

At 1500 UTC the region with DS surface winds encompassed the smallest area relative to the entire analysis period (Fig. 3a) for both the CLEAN and POLLUTED simulations. After 1400 UTC, the convective region of the MCS began to diminish and the storm became dominated by stratiform precipitation (Figs. 9 and 11, Part I), indicating the onset of MCS dissipation. During the intensification stage of the storm, an increase in aerosol number concentrations introduced a monotonic response in the derecho characteristics where the increase in aerosol concentrations produced stronger DS winds over a smaller region in comparison to the CLEAN simulation. In contrast, at 1500 UTC, the increase in aerosol number concentrations led to a non-monotonic response in both DS strength and area. Relative to the CLEAN simulation, a moderate increase in aerosol concentration (POLLUTED) decreased the DS wind area by 36% (Fig. 3a) as well as the magnitude of the DS winds (Figs. 3b and 4c), while a greater increase in aerosol concentration (5xPOLLUTED) produced DS winds over an area 200% larger (Fig. 3a) with similar DS wind intensity (Figs. 3b and 4c). The location of the DS winds at 1500 UTC for all three cases are superimposed on the surface density potential temperature in Fig. 10, which is representative of the location of the cold pool and hence the gust front. At this time, all three simulations produced DS winds in close proximity to a meso-γ vortex (outlined in green contours of relative vertical vorticity in Fig. 10) at the leading edge of the gust front. The location of a meso-γ vortex at the gust front in this study is supported by observations (Weisman and Trapp, 2003), observations for the 8 May 2009 MCS in particular (Przybylinksi et al., 2010), and a recent numerical simulation of the MCS (Xu et al., 2015b). For both the CLEAN (Fig. 11a) and 5xPOLLUTED (Fig. 11c) simulations, two BT flows are apparent: the RIJ and the UDD, while the BT flow only follows a RIJ for the POLLUTED simulation (Fig. 11b). Comparisons of the characteristics of the RIJ in the three simulations are shown in Fig. 12. The RIJ was similar in both the intensity and elevation in the CLEAN and POLLUTED simulations. Therefore, the smaller area with DS winds, as well as the weaker DS winds, in the POLLUTED simulation, appears to be explained by the lack of an UDD within this simulation.

As seen in Section 4.1, the intensity of a meso-γ vortex impacts the UDD. Therefore, in order to understand why the POLLUTED simulation did not form a UDD flow regime, the intensity of the meso-γ vortex was compared among the simulations. This was done by examining the maximum vertical relative vorticity within the meso-γ vortex (Fig. 13a), identified as a 3D volume where values of relative vertical vorticity are at least 0.01 s^{-1}, in keeping with previous studies (e.g. Weisman and Trapp, 2003). The maximum updraft velocity and minimum perturbation Exner function were examined in Fig. 13b and c, respectfully. The column mean of the maximum relative vertical vorticity was 0.02, 0.015 and 0.017 s^{-1} in the 5xPOLLUTED, POLLUTED and CLEAN simulations, respectively. Furthermore, the meso-γ vortex in the 5xPOLLUTED simulation was 3 km deeper in comparison to both CLEAN and POLLUTED. Therefore, the strongest meso-γ vortex (Fig. 13a) occurred in the 5xPOLLUTED simulation, followed by the CLEAN, and the weakest meso-γ vortex occurred in the POLLUTED simulation. The weaker meso-γ vortex within the POLLUTED simulation did not result in the development of an UDD and this flow regime could not contribute to the DS winds at the surface. In order to fully understand how changes in aerosol concentrations led to the non-monotonic trend in the development of the meso-γ vortices, vorticity budget analyses needs to be conducted. This is left for future work.

The UDD flow characteristics between the CLEAN and 5xPOLLUTED simulations is further examined by comparing the horizontal wind speeds of the parcels as they descended to the surface following the UDD (Fig. 14). In the 5xPOLLUTED simulation the parcels entered the meso-γ vortex with a higher horizontal velocity (Fig. 14b). Therefore, the higher horizontal velocities of the parcels at higher altitudes led to the formation of DS winds at the surface indicating that the transfer of horizontal momentum from higher levels contributed to the formation of the DS winds. In contrast, in the CLEAN simulation, parcels entered the meso-γ vortex at both lower altitudes and lower horizontal wind speeds (Fig. 14a). The parcels accelerated to DS winds only after descending to the surface. The near surface acceleration within the CLEAN simulation is explained by higher evaporation rates, which is seen by the lower density potential temperatures (Fig. 10). As was shown in part I, the 5xPOLLUTED simulation produced larger rain droplets at this time. These droplets evaporated less readily thereby enhancing the amount of precipitation reaching the surface and decreasing the

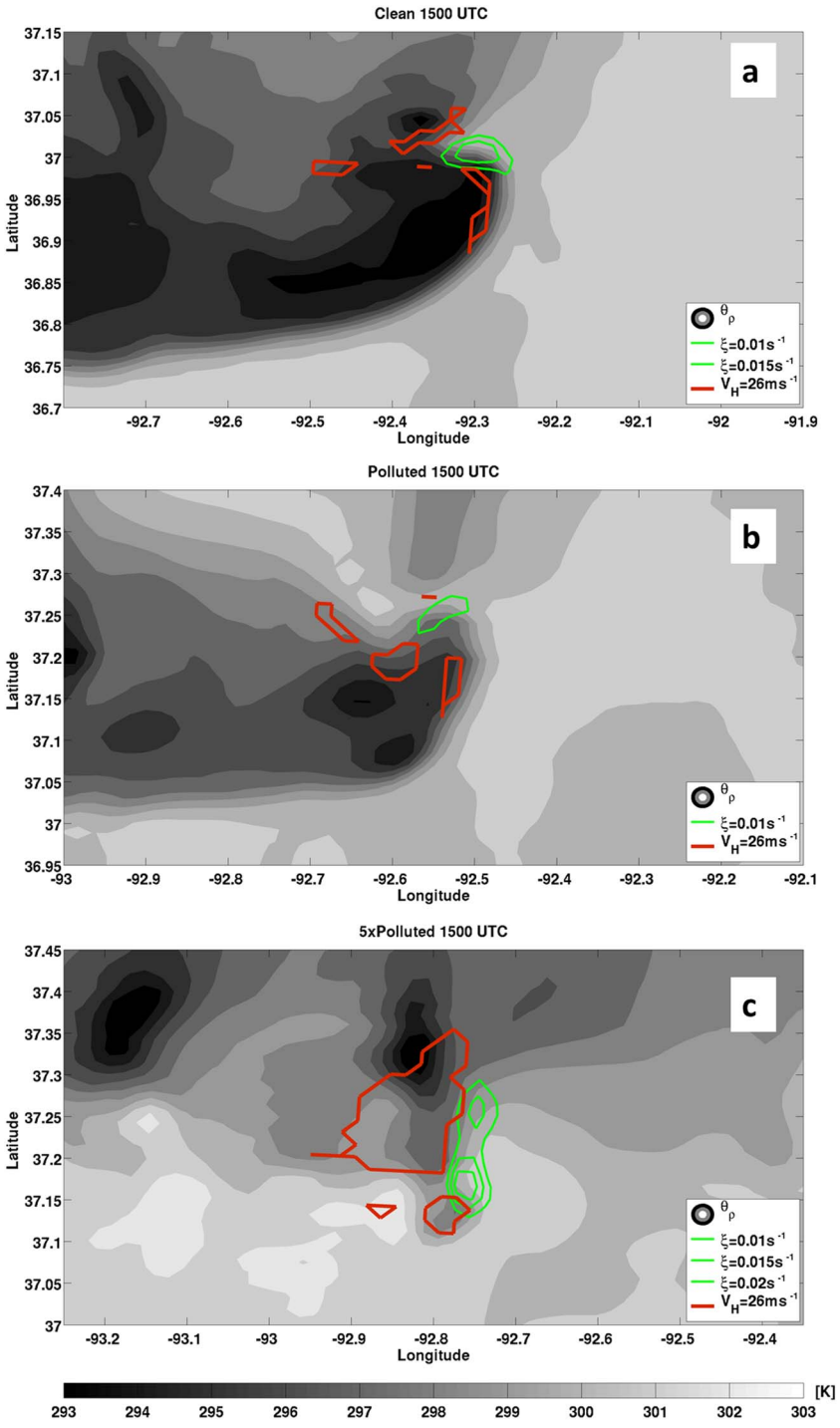

Fig. 10. Surface density potential temperature (shaded), locations of DS winds (contoured in red) and the mesovortex at 1 km AGL (contoured in green) are presented for the Clean (a), Polluted (b) and 5xPolluted (c) simulations at 1500 UTC. (For interpretation of the references to colour in this figure legend, the reader is referred to the web version of this article.)

evaporation potential. The horizontal acceleration of the UDD at higher levels within the 5xPOLLUTED simulation is explained by a larger horizontal pressure gradient force induced by the lower pressure within the stronger meso-γ vortex (Fig. 13c).

5. Discussion

The sensitivity of the 8 May 2009 derecho to aerosol loading has been investigated by numerically simulated the storm and conducting three simulation in which aerosol number concentrations differed. Due to the complex nature of the dynamics of an MCS, identifying the impact of increased aerosols on the strength of the near surface convective outflow is challenging. This is because aerosols serving as CCN were found in this study to modify the strength of a derecho in the following three ways: (Adams-Selin et al., 2013) directly modifying the intensity of the downdrafts due to phase changes of hydrometeors; (Andreae et al., 2004) indirectly modifying the relationship between the horizontal vorticity generated in association with the environmental shear and that baroclinically-generated by the storm-produced cold pool; and (Atkins and St. Laurent, 2009a) modification of the strength of the mesovortex due to changes in vertical relative vorticity.

Previous numerical studies have shown that mesoscale storm dynamics and longevity are sensitive to changes in hydrometeor diameters through changes to the melting and evaporation rates, and thus, the strength of the storm-produced cold pool. van den Heever and Cotton (2004) found that decreasing hail diameter sizes increased cold pool

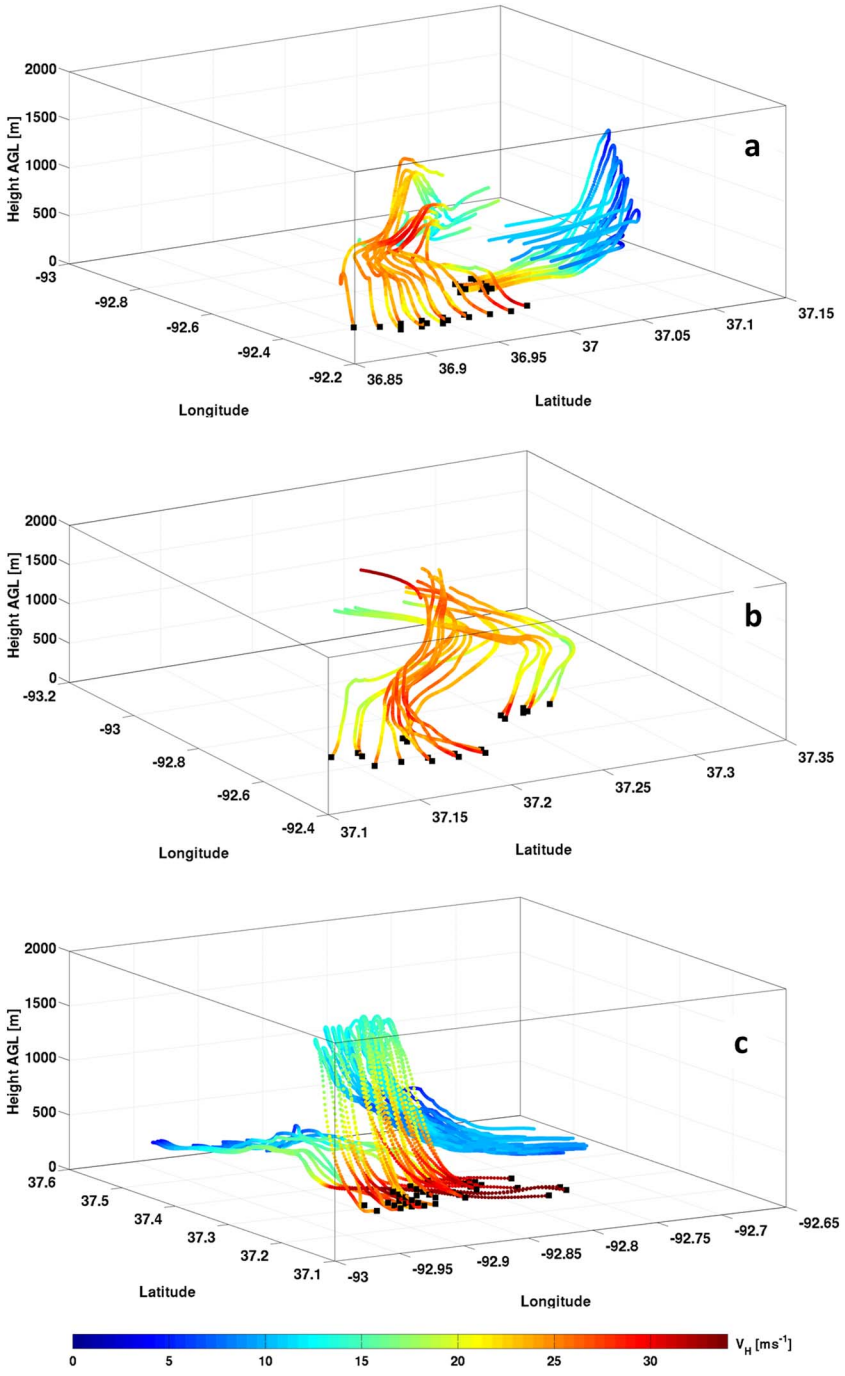

Fig. 11. 1500 UTC sample 3D back-trajectory plots during 30 min for the (a) Clean, (b) Polluted and (c), 5xPolluted simulations. Trajectories are colored according to the parcel's horizontal wind speeds. Origins of the back-trajectories (at 1500 UTC, near the surface) are noted by the black square marker.

strength due to an increase in melting and subsequent evaporation. Smaller hail hydrometeors increase the melting potential due to smaller terminal fall speeds and an increase in the integrated surface area exposed to melting. Similarly, Adams-Selin et al. (2013) found cold pool intensity to vary as a function of graupel size and density. Both studies demonstrated that smaller ice hydrometeors led to stronger cold pools. In Part I of this study, increases in aerosol concentration were found to produce larger rain drops and hail stones which contributed to an enhancement in the amount of convective precipitation produced by the storm. The smaller rain and hail diameters within the CLEAN simulation produces the stronger cold pools found in Part II of this study. However, the strength of the cold pool was found to be sensitive to both the size of the precipitating hydrometers as well as precipitation rates. During the intensification stage of the MCS, the strongest cold pool was found in the CLEAN simulation followed by the 5xPOLLUTED simulation, and the weakest cold pool evident in the POLLUTED simulation. This was attributed to higher rain rates in the 5xPOLLUTED simulation which yielded more hydrometeor mass available to be melted and evaporated. During the dissipation stage of the MCS, when the differences in the convective rain rates were smaller among the simulations, a monotonic trend was found where increased aerosol concentrations formed weaker cold pools due to the larger precipitating hydrometers. The changes in cold pool strength modify the formation of Derecho-Strength (DS) winds at the surface by impacting the formation of the RIJ (Weisman, 1992), as well as the strength of meso-γ vortices at the gust front (Atkins and St. Laurent, 2009b).

In order to understand the impact of aerosol loading on the simulated derecho in this case study, back trajectory analysis from the locations with DS winds at the surface were performed for all three of the simulations during two stages of the simulated MCS: intensification and

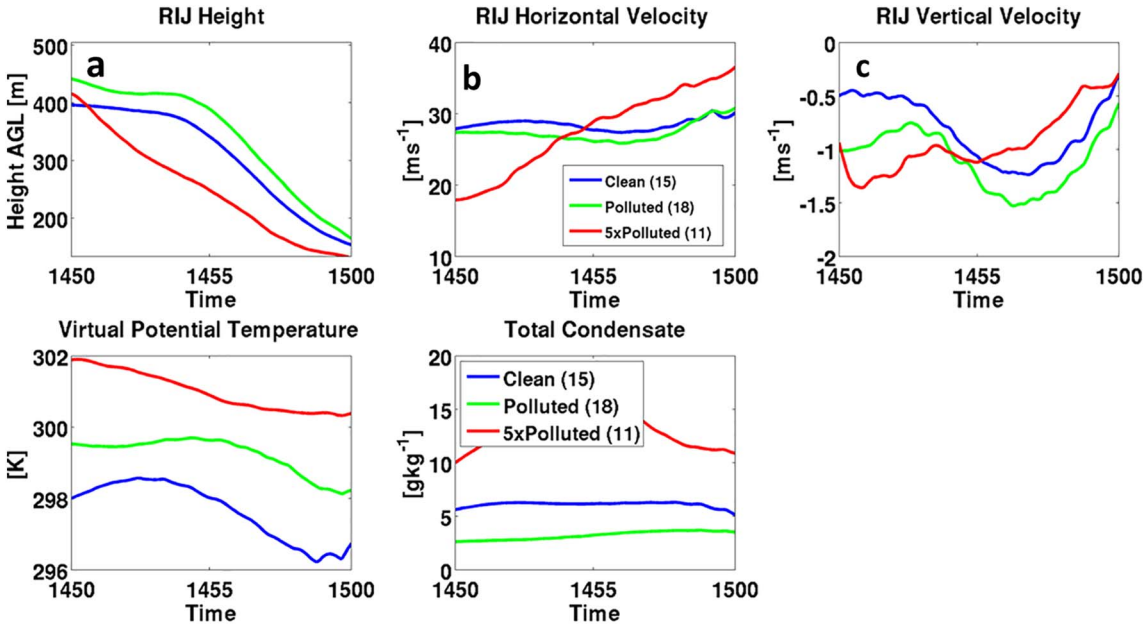

Fig. 12. 1500 UTC mean back trajectory parcel characteristics of (a) height, (b) horizontal velocity and (c) vertical velocity for the Clean (blue), Polluted (green) and 5xPolluted (red) simulations during the last 10 min of the parcels descent. Numbers in the brackets within the legend represent the number of parcels following the RIJ BT flow. (For interpretation of the references to colour in this figure legend, the reader is referred to the web version of this article.)

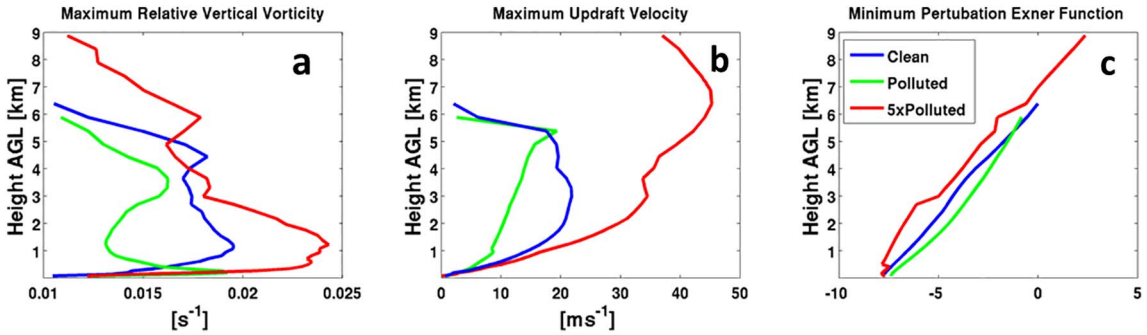

Fig. 13. Characteristics of the Mesovortex (within a region of relative vertical vorticity > 0.01 s^{-1} (a) maximum relative vertical vorticity, (b) maximum updraft velocity and the (c) minimum Exner perturbation function with height for the three simulations: Clean (blue), Polluted (green) and 5xPolluted (red). (For interpretation of the references to colour in this figure legend, the reader is referred to the web version of this article.)

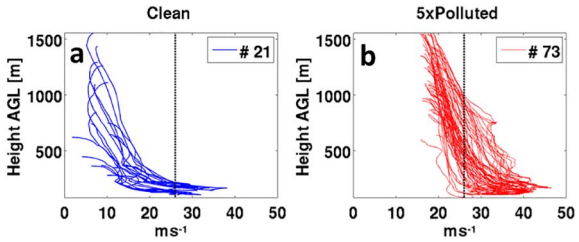

Fig. 14. Horizontal wind speed of parcels during the decent following the UDD for the Clean (left) and 5xPolluted simulations (right). Numbers in the legend represent the number of parcels plotted, determined by the region in Fig. 11a and c.

dissipation. Results of the BT analysis suggested that two types of air flows contributed to the formation of the DS winds: (Adams-Selin et al., 2013) a rear inflow jet (RIJ) and (Andreae et al., 2004) downdrafts following an up-down downdraft (UDD) trajectory associated with a meso-γ vortex. The findings that the DS winds were generated by both a RIJ and flow associated with a meso-γ vortex is consistent with the findings of Atkins and St. Laurent (2009b). Furthermore, the findings of air parcels "originating" within the boundary layer contribution to the formation of DS following a trajectory of an UDD is consistent with previous findings (Knupp, 1987; Bernardet and Cotton, 1998). A schematic summarizing the 3D flow driving the DS winds within the

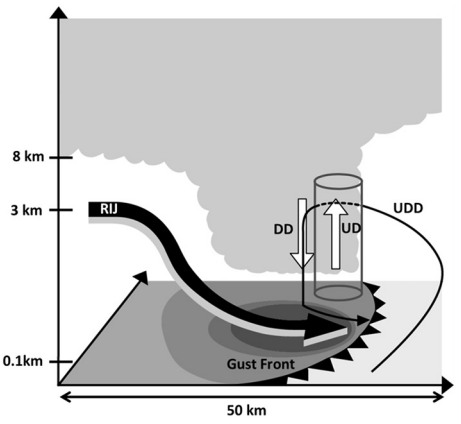

Fig. 15. Schematic depiction summarizing the 3D flow of the Rear-Inflow Jet (RIJ) and Up-down downdraft (UDD), the meso-γ vortex at the gust relative to the location of the cold pool (shaded in the X-Y plan) and gust front, the convective updraft (UD) and precipitating convective downdraft (DD).

simulated 8 May 2009 derecho event is presented in Fig. 15 derived from the back-trajectory analysis conducted in this study. The flow following the UDD reaches the surface south of the meso-γ vortex,

similar to the findings of Atkins and St. Laurent (2009b). It is important to note that the RIJ captured in the 60 min back trajectory flow is focused near (~50 km) ** of ** the convective line and does not include the entire extent of the RIJ which extends several hundred kilometers behind the convective line, as seen in Johnson and Hamilton (1988).

A time dependent signal was found between the derecho strength and aerosol loading due to the dynamics which produced the simulated derecho event. During the intensification stage of MCS, the aerosol-induced changes in the precipitation formation, shown in Part I, impacted the balance between the horizontal vorticity generated by the cold pool and that of the low-level environmental wind shear (Rotunno et al., 1988). In this study, this balance was found to be sensitive to aerosol loading through their impact on cold pool strength, which in turn, modified the predominant flow which produced the DS winds at the surface from a descending RIJ (in the CLEAN simulation) to an UDD (in the 5xPOLLUTED simulation). In the latter case, the weaker cold pool was associated with a more upright oriented convective updraft, and a stronger meso-γ vortex. As the storm matured, the changes in aerosol concentrations impacted the derecho event by altering the intensity the meso-γ vortex and a non-monotonic trend with increase in aerosol concentrations was observed, where the derecho event weakened only within the moderately polluted simulation. Based on previous research, it is hypothesized here that these changes in the cold pool affected the strength of the moeso-γ vortex by altering the amount of baroclinically-generated horizontal vorticity which was made available to be tilted into the vertical (e.g. van den Heever and Cotton, 2004) and the fraction of horizontal vorticity tilted into the vertical (Atkins and St. Laurent, 2009a). To confirm this, a vorticity budget analysis should be conducted as part of future work. Besides impacting the amount of horizontal relative vorticity which is made available to be tilted into the vertical (e.g. van den Heever and Cotton, 2004), a meso-γ vortex can be intensified by the generation of vertical relative vorticity due to stretching within a rotating updraft which is a function of the updraft speeds (Atkins and St. Laurent, 2009a). Since changes in aerosol number concentrations affect the redistribution of latent heat within the storm and subsequently the updraft speeds (Andreae et al., 2004; Khain et al., 2005; Koren et al., 2005; van den Heever and Cotton, 2007; Li et al., 2009; Rosenfeld et al., 2008; Storer and van den Heever, 2013; Tao et al., 2012; Storer and van den Heever, 2013), these changes could be expected to impact meso-γ vortex intensity. Indeed, in this study, it was found that changes in aerosol concentration did impact updraft speeds (Fig. 19, Part I) and the meso-γ vortex intensity.

6. Conclusions

The microphysical effects of increased aerosol concentrations on the characteristics and intensity of a derecho were examined in this study by performing a numerical analysis of an MCS case study using a mesoscale cloud resolving model, RAMS. The case study chosen was the 8 May 2009 “Super-derecho” MCS. A set of three RAMS sensitivity simulations was conducted in which the aerosol distribution, number concentration and chemical composition differed based on the output of a 3D chemical model, GEOS-Chem. The CLEAN simulation contained only aerosol concentrations from non-anthropogenic sources, the POLLUTED included aerosols from both anthropogenic and non-anthropogenic sources and the 5xPOLLUTED had the same distribution as in the POLLUTED simulation, but multiplied by a factor of five. Back trajectory analysis from grid points with derecho-strength winds were performed for two periods within the storm: the intensification and dissipation stages. Analysis of the sensitivity of the simulated derecho event to changes in aerosol concentration shows the following:

- Changes in aerosol concentrations did not significantly impact the MCS longevity, total precipitation or the formation of the derecho, however it did impact the distribution of convective vs. stratiform precipitation (Part I) and the derecho characteristics (intensity and area).
- Two air flows were found to produce the derecho event: a rear inflow jet (RIJ) and an up-down downdraft (UDD) associated with a meso-γ vortex at the gust front.
- Aerosols acting as CCN were found to impact the derecho intensity directly by modifying the cold pool strength and downdraft speeds, and indirectly by altering the balance between the horizontal vorticity generated by the cold pool and that of the environment, as well as the characteristics of the meso-γ vortex at the gust front.
- During the MCSs' intensification stage, an increase in aerosol concentration resulted in a shift in the flow regime from being dominated by the RIJ to that of a downburst following the pathway of an up-down downdraft, which exhibited stronger surface winds speeds over a smaller area.
- During the MCSs' dissipation stage, the changes in the derecho characteristics were attributed to the up-down downdraft associated with the meso-γ vortex in all three simulations. At this time, acceleration within the up-down downdraft in the highly polluted simulation was attributed to enhanced horizontal acceleration at higher altitudes as the flow approached the stronger meso-γ vortex. Within the cleaner simulation, the flow was accelerated near the surface due to higher evaporation rates of hydrometeors. The meso-γ vortex at this time was the weakest within the moderately polluted simulation and did not produce an up-down downdraft which could contribute to derecho-strength winds at the surface.

The findings of this study are limited to the environment of this case study which included a strong and deep LLJ (Coniglio et al., 2011) and anomalously high PW values which supported enhanced convective precipitation with increased aerosol concentration. The non-monotonic trends in the derecho characteristics with increased aerosol concentrations found in this study should be examined for other case studies with varying humidity.

Acknowledgements

The authors wish to thank Dr. Jeffery Pierce for providing the GOES-Chem aerosol data used in this study and Stephen Saleeby for his suggestions and input in simulating the 8 May 2009 case study MCS. This work was funded by the National Science Foundation under grant AGS-1005041.

References

Adams-Selin, R.D., van den Heever, S.C., Johnson, R.H., 2013. Impact of graupel parameterization schemes on idealized bow echo simulations. Mon. Weather Rev. 141, 1241–1262.
Andreae, M.O., Rosenfeld, D., Artaxo, P., Costa, A.A., Frank, G.P., Longo, K.M., Silva-Dias, M.A.F., 2004. Smoking rain clouds over the Amazon. Science 303, 1337–1342.
Atkins, N.T., St. Laurent, M., 2009a. Bow echo mesovortices. Part II: their Genesis. Mon. Weather Rev. 137, 1514–1532.
Atkins, N.T., St. Laurent, M., 2009b. Bow echo mesovortices. Part I: processes that influence their damaging potential. Mon. Weather Rev. 137, 1497–1513.
Bernardet, L.R., Cotton, W.R., 1998. Multiscale evolution of a derecho-producing mesoscale convective system. Mon. Weather Rev. 126, 2991–3015.
Bey, I., Jacob, D.J., Yantosca, R.M., Logan, J.a., Field, B.D., Fiore, A.M., Li, Q.-B., Liu, H.-Y., Mickley, L.J., Schultz, M.G., 2001. Global modeling of tropospheric chemistry with assimilated meteorology: model description and evaluation. J. Geophys. Res. 106, 73–95.
Bryan, G.H., Morrison, H., 2012. Sensitivity of a simulated squall line to horizontal resolution and parameterization of microphysics. Mon. Weather Rev. 140, 202–225.
Charba, J., 1974. Application of gravity current model to analysis of squall-line gust front. Mon. Weather Rev. 102 (2), 140–156.
Coniglio, M.C., Corfidi, S.F., Kain, J.S., 2011. Environment and early evolution of the 8 May 2009 derecho-producing convective system. Mon. Weather Rev. 139, 1083–1102.
Coniglio, M.C., Corfidi, S.F., Kain, J.S., 2012. Views on applying RKW theory: an illustration using the 8 May 2009 derecho-producing convective system. Mon. Weather Rev. 140, 1023–1043.
Cotton, W.R., Pielke Sr., R.A., Walko, R.L., Liston, G.E., Tremback, C.J., Jiang, H., McAnelly, R.L., Harrington, J.Y., Nicholls, M.E., Carrio, G.G., McFadden, J.P., 2003. RAMS 2001: current status and future directions. Meteorog. Atmos. Phys. 82, 5–29.

Emanuel, K.A., 1994. Atmospheric Convection. Oxford University.
Evans, C., Weisman, M.L., Bosart, L.F., 2014. Development of an intense, warm-core mesoscale vortex associated with the 8 May 2009 “Super Derecho” convective event. J. Atmos. Sci. 71, 1218–1240.
Fan, J., Leung, L.R., Rosenfeld, D., Chen, Q., Li, Z., Zhang, J., Yan, H., 2013. Microphysical effects determine macrophysical response for aerosol impacts on deep convective clouds. Proc. Natl. Acad. Sci. U. S. A. 110, E4581–E4590.
Fujita, T.T., 1978. Manual of downburst identi_cation for project NIMROD. In: Technical Report. Dept. of Geophysical Sciences, University of Chicago, Chicago, IL.
Fujita, T.T., Wakimoto, R.M., 1981. Five scales of airflow associated with a series of downbursts on 16 July 1980. Mon. Weather Rev. 109, 1438–1456.
Grant, L.D., van den Heever, S.C., 2015. Cold pool and precipitation responses to aerosol loading: modulation by dry layers. J. Atmos. Sci. 72, 1398–1408.
Grasso, L.D., 1996. Numerical Simulation of the May 15 and April 26, 1991 Tornadic Thunderstorm. (Ph.D. dissertation) Colorado State University (151 pp. [Available from Department of Atmospheric Science, Colorado State University, Fort Collins, CO 80523]).
van den Heever, S.C., Cotton, W.R., 2004. The impact of hail size on simulated supercell storms. J. Atmos. Sci. 61, 1596–1609.
van den Heever, S.C., Cotton, W.R., 2007. Urban aerosol impacts on downwind convective storms. J. Appl. Meteorol. Climatol. 46, 828–850.
Hinrichs, G., 1888. Am. Meterological J. 1, 306–317.
Houze Jr, R.A., Biggerstaff, M.I., Rutledge, S.A., Smull, B.F., 1989. Interpretation of doppler weather radar displays of midlatitude mesoscale convective systems. Bull. Am. Meteorol. Soc. 70 (6), 608–619.
Johns, R.H., 1982. A synoptic climatology of northwest flow severe weather outbreaks. Part I: nature and significance. Mon. Weather Rev. 110, 1653–1663.
Johns, R.H., Hirt, W.D., 1987. Derechos: widespread convectively induced windstorms. Weather Forecast. 2, 32–49.
Johnson, R.H., Hamilton, P.J., 1988. The relationship of surface pressure features to the precipitation and airflow structure of an intense midlatitude squall line. Mon. Weather Rev. 116, 1444–1473.
Keene, K.M., Schumacher, R.S., 2013. The bow and arrow mesoscale convective structure. Mon. Weather Rev. 141, 1648–1672.
Khain, A., Rosenfeld, D., Pokrovsky, A., 2005. Aerosol impact on the dynamics and microphysics of deep convective clouds. Q. J. R. Meteorol. Soc. 131, 2639–2663.
Klimowski, B.A., Hjelmfelt, M.R., Bunkers, M.J., 2004. Radar observations of the early evolution of bow echoes. Weather Forecast. 19, 727–734.
Knupp, K.R., 1987. Downdrafts within High Plains Cumulonimbi. Part I: general kinematic structure. J. Atmos. Sci. 44 (6), 987–1008.
Koren, I., Kaufman, Y.J., Rosenfeld, D., Remer, L.A., Rudich, Y., 2005. Aerosol invigoration and restructuring of Atlantic convective clouds. Geophys. Res. Lett. 32, 1–4.
Lebo, Z.J., Morrison, H., 2014. Dynamical effects of aerosol perturbations on simulated idealized squall lines. Mon. Weather Rev. 142, 991–1009.
Lee, S.S., Donner, L.J., Phillips, V.T.J., Ming, Y., 2008. Examination of aerosol effects on precipitation in deep convective clouds during the 1997 ARM summer experiment. Q. J. R. Meteorol. Soc. 134, 1201–1220.
Li, G., Wang, Y., Lee, K.H., Diao, Y., Zhang, R., 2009. Impacts of aerosols on the development and precipitation of a mesoscale squall line. J. Geophys. Res. Atmos. 114, 1–18.
Newton, C.W., 1950. Structure and mechanism of the prefrontal squall line. J. Meteorol. 7 (3), 210–222.
Orlanski, I., 1975. A rational subdivision of scales for atmospheric processes. Am. Meteorol. Soc. 56, 527–530.
Parker, M.D., Johnson, R.H., 2000. Organizational modes of midlatitude mesoscale convective systems. Mon. Weather Rev. 128, 3413–3436.
Przybylinksi, R.W., Schaumann, J.S., Cramer, D.T., Atkins, N.T., 2010. The 08 May 2009 Missouri derecho: radar analysis and warning implications over parts of Southwest Missouri. In: 25th Conf. on Severe Local Storms, Denver, CO, Amer. Meteor. Soc., 3B.1.
Rosenfeld, D., Lohmann, U., Raga, G.B., O'Dowd, C.D., Kulmala, M., Fuzzi, S., Reissell, A., Andreae, M.O., 2008. Flood or drought: how do aerosols affect precipitation? Science 321, 1309–1313.
Rotunno, R., Klemp, J.B., Weisman, M.L., 1988. A theory for strong, long-lived squall lines. J. Atmos. Sci. 45 (3), 463–485.
Saleeby, S.M., van den Heever, S.C., 2013. Developments in the CSU-RAMS aerosol model: emissions, nucleation, regeneration, deposition, and radiation. J. Appl. Meteorol. Climatol. 52, 2601–2622.
Saleeby, S.M., Heever, S.C., Marinescu, P.J., Kreidenweis, S.M., DeMott, P.J., 2016. Aerosol effects on the anvil characteristics of mesoscale convective systems. J. Geophys. Res. 121.
Schmidt, J.M., Cotton, W.R., 1989. A High Plains squall line associated with severe surface winds. J. Atmos. Sci. 46 (3), 281–302.
Seigel, R.B., van den Heever, S.C., 2013. Squall-line intensification via hydrometeor recirculation. J. Atmos. Sci. 70, 2012–2031.
Seigel, R.B., van den Heever, S.C., Saleeby, S.M., 2013. Mineral dust indirect effects and cloud radiative feedbacks of a simulated idealized nocturnal squall line. Atmos. Chem. Phys. 13, 4467–4485.
Smull, B.F., Houze, R.A., 1987. Rear inflow in squall lines with trailing stratiform precipitation. Mon. Weather Rev. 115, 2869–2889.
Storer, R.L., van den Heever, S.C., 2013. Microphysical processes evident in aerosol forcing of tropical deep convective clouds. J. Atmos. Sci. 70, 430–446.
Tao, W.-K., Li, X., Khain, A., Matsui, T., Lang, S., Simpson, J., 2007. Role of atmospheric aerosol concentration on deep convective precipitation: cloud-resolving model simulations. J. Geophys. Res. 112.
Tao, W.K., Chen, J.P., Li, Z., Wang, C., Zhang, C., 2012. Impact of aerosols on convective clouds and precipitation. Rev. Geophys. 50 (2).
Tompkins, A.M., 2001. Organization of tropical convection in low vertical wind shears: the role of cold pools. J. Atmos. Sci. 58, 1650–1672.
Wakimoto, R.M., Murphey, H.V., Davis, C.A., Atkins, N.T., 2006. High winds generated by bow echoes. Part II: the relationship between the mesovortices and damaging straight-line winds. Mon. Weather Rev. 134, 2813–2829.
Weisman, M.L., 1992. The role of convectively generated rear-inflow jets in the evolution of long-lived mesoconvective systems. J. Atmos. Sci. 49 (19), 1826–1847.
Weisman, M.L., 1993. The genesis of severe, long-lived bow echoes. J. Atmos. Sci. 50, 645–670.
Weisman, M.L., Trapp, R.J., 2003. Low-level mesovortices within squall lines and bow echoes. Part I: overview and dependence on environmental shear. Mon. Weather Rev. 131, 2804–2823.
Weisman, M.L., Evans, C., Bosart, L., 2013. The 8 May 2009 superderecho: analysis of a real-time explicit convective forecast. Weather Forecast. 28, 863–892.
Xu, X., Xue, M., Wang, Y., 2015a. Mesovortices within the 8 May 2009 bow echo over the Central United States: analyses of the characteristics and evolution based on Doppler radar observations and a high-resolution model simulation. Mon. Weather Rev. 143, 2266–2290.
Xu, X., Xue, M., Wang, Y., 2015b. The genesis of mesovortices within a real-data simulation of a bow echo system. J. Atmos. Sci. 72, 1963–1986.